

Generation and robustness of non-local correlations induced by Heisenberg XYZ and intrinsic decoherence models: (x, y) -spin-orbit interactions and x - magnetic field

F. Aljuaydi,^{1,*} S. N. Almutairi,¹ and A.-B. A. Mohamed^{1,2}

¹*Department of Mathematics, College of Science and Humanities,
Prince Sattam bin Abdulaziz University, Al Kharj 11942, Saudi Arabia*

²*Department of Mathematics, Faculty of Science, Assiut University, Assiut, Egypt*

In this work, the Milburn intrinsic decoherence model is used to investigate the role of spin-spin Heisenberg-XYZ interaction supported by spin-orbit Dzyaloshinsky–Moriya (DM) interactions of x and y -directions together in the non-local correlation (NLC) dynamics of Local quantum Fisher information (LQFI), local quantum uncertainty (LQU), and Log-negativity’s entanglement. The two-qubit-Heisenberg-XYZ (non-X)-states’ non-local correlation generations are explored under the effects of the uniformity and the inhomogeneity of an applied x -direction external inhomogeneous magnetic field (EIMF). Our meticulous exploration of the obtained results shows that the spin-spin Heisenberg XYZ and x, y -spin-orbit interactions have a high capability to raise non-local correlations in the presence of a weak external magnetic field. The raised non-local correlation can be improved by strengthening the spin-spin and x, y -spin-orbit interactions and increasing the EIMF’s inhomogeneity and uniformity. Non-local correlation oscillations’ amplitudes and fluctuations are increased. The degradations of the NLCs’ generations in the presence of intrinsic decoherence (NLCs’ robustness against intrinsic decoherence) can be decreased by strengthening the spin-spin interactions. They can be increased by increasing the intensities of x, y -spin-orbit interactions as well as increasing the EIMF’s inhomogeneity and uniformity.

Keywords: non-local correlation; Heisenberg XYZ states; magnetic fields: spin-orbit interaction

I. INTRODUCTION

Among the numerous quantum systems proposed to implement quantum information and computation [1, 2], superconducting circuits, trapped ions, and semiconductor quantum dots are essential techniques for realizing quantum bits (qubits). Based on electron spins trapped in quantum dots, a quantum computer protocol has been initially proposed [3–5], the electron having a spin of $1/2$ is the simplest natural qubit. Recently, quantum computation (as a single-spin-qubit geometric gate) with electron spins (single-spin-qubit geometric gate) has been realized in quantum dots [6, 7]. Due to tunneling the electrons from one to the other, the spin-spin coupling and spin-orbit coupling of the interaction between two qubits can be realized by considering a two-qubit system represented by two coupled quantum dots’ two electrons. Therefore, Heisenberg XYZ models describing spin-spin interactions are among of the important proposed qubit systems. Two qubit Heisenberg XYZ models have been realized in different systems, including bosonic atoms inside an optical lattice [8], trapped ions [9] and superconductor systems [10], and linear molecules [11]. Heisenberg XYZ models have been updated to include spin-orbit interactions [12, 13] with the first order of SO coupling (that is known by Dzyaloshinsky–Moriya interactions [14] (realizing by an antisymmetric superexchange La_2CuO_4 interaction [15]), the second order of SO coupling (Kaplan-Shekhtman-Entin-Wohlman-Aharony interaction [16]). Spin- $1/2$ Heisenberg XYZ models also have been updated to include dipole-dipole interaction [17], and inhomogeneous external magnetic fields (IEMFs) [18, 19].

Exploring two-qubit information dynamics in different proposed qubit systems to two-qubit resources, relating to different types of nonlocal correlations (as entanglement, quantum discord, ...), is one of the most required research fields in implementing quantum information and computation [20]. Quantum entanglement (QE) (realizing by quantifiers’ entropy [21], concurrence [22], negativity, and log-negativity [23], ...) is an important type of qubits’ nonlocal correlations (NLCs) [24, 25] and applications have an important role in quantum information fields. Where QE has a wide range of applications in implementing quantum computation, teleportation [26, 27], quantum optical memory [28], and quantum key distribution [29]. After implementing quantum discord as another type of qubits’ NLCs beyond entanglement [30], several NLCs’ quantifiers have been introduced to address other NLCs [31, 32] by using Wigner–Yanase (WY) skew information [33] and quantum Fisher information (QFI) [34]. Where, WY-skew-information minimization (local quantum uncertainty [35] LQU) and the WY-skew-information maximization (uncertainty-induced nonlocality [36]) have been introduced to quantify other NLCs beyond entanglement. Also, the minimization of QFI (local quantum Fisher information, LQFI) was used to implementing other qubits’ NLCs [37, 38]. LQU has a direct connection to LQFI [39, 40], establishing more two-qubit NLCs in several proposed qubit systems [46, 47]: as hybrid-spin systems (under random noise [41] and intrinsic decoherence [42]), two-coupled double quantum dots [43], the mixed-spin Heisenberg [44], Heisenberg XXX system [45].

The information dynamics of the two-spin Heisenberg XYZ states have been investigated, by using Milburn intrinsic decoherence model [48], of entanglement teleportation based on the Heisenberg XYZ chain [49, 50], Fisher of Heisenberg XXX states’ LQFI beyond IEMF effects [51], quantum cor-

* Corresponding author: f.aljuaydi@psau.edu.sa

relations of concurrence and LUQ [52]. The previous works have focused on exploring the time evolution of the two-spin Heisenberg-XYZ states' NLCs with limited conditions on the spin-spin and spin-orbit interactions, and the applied magnetic fields, to ensure residing two-qubits X-states [53–61]. Therefore, by using the Milburn intrinsic decoherence and Heisenberg XYZ models are used to investigate the non-local correlation dynamics of LQFI, LQU, and log-negativity (LN) for general two-qubit-Heisenberg-XYZ (non-X)-states, inducing by other specific conditions on the spin-spin and spin-orbit interactions, as well as the applied magnetic fields.

The manuscript structure is prepared to include the Milburn intrinsic decoherence equation including the Heisenberg XYZ model and its solution in Sec. (II). But in Sec. (III), we introduce the definition of the NLCs' quantifiers of LQFI, LQU, and LN. Sec. (IV) presents the outcomes of the dependence of the NLCs' quantifiers on the physical parameters. Our conclusions are provided in Sec. (V).

II. THE HEISENBERG SPIN MODEL

Here, Milburn intrinsic decoherence model and Heisenberg XYZ model are used to examine the embedded capabilities in spin-spin interaction and spin-orbit interaction (that describes Dzyaloshinsky–Moriya (DM) x, y -interactions with the first order of SO couplings D_x and D_y) to generate essential two SO-qubits' nonlocal correlations (NCs) under the effects of the uniformity B_m and the inhomogeneity b_m of applied external inhomogeneous magnetic field (EIMF). For two spin-qubits (each k -qubit ($k = A, B$) is described by upper $|1_k\rangle$ and lower $|0_k\rangle$ states), the Hamiltonian of the system is written as

$$\hat{H} = \sum_{\alpha=x,y,z} J_{\alpha} \hat{\sigma}_A^{\alpha} \hat{\sigma}_B^{\alpha} + \sum_{k=A,B} \vec{B}_k \cdot \vec{\sigma}_k + \vec{D} \cdot (\vec{\sigma}_A \times \vec{\sigma}_B). \quad (1)$$

$\vec{\sigma}_k = (\hat{\sigma}_k^x, \hat{\sigma}_k^y, \hat{\sigma}_k^z)$ with $\hat{\sigma}_k^{x,y,z}$ represent the k -qubit Pauli matrices. $\vec{B}_k = (B_k^x, B_k^y, B_k^z)$ is the vector of the external magnetic field applying on k -spin, $\vec{B}_k \cdot \vec{\sigma}_k = B_k^x \hat{\sigma}_k^x + B_k^y \hat{\sigma}_k^y + B_k^z \hat{\sigma}_k^z$. In our work, we consider that the EIMF is applied only in the x -direction: $\vec{B}_k = (B_k^x, 0, 0)$, $B_A^x = B_m + b_m$, and $B_B^x = B_m - b_m$. $\vec{D} = (D_x, D_y, D_z)$ is the spin-orbit/DM interaction vector. Therefore, we have $\vec{D} \cdot (\vec{\sigma}_A \times \vec{\sigma}_B) = D_x \hat{C}_x + D_y \hat{C}_y + D_z \hat{C}_z$ with $\hat{C}_{\alpha} = \hat{\sigma}_A^{\alpha+1} \hat{\sigma}_B^{\alpha+2} - \hat{\sigma}_A^{\alpha+2} \hat{\sigma}_B^{\alpha+1}$ ($\alpha = x, y, z$).

Here, we take only the x, y -spin-orbit interactions: $\vec{D} = (D_x, D_y, 0)$. The capacitive spin-spin and x, y -spin-orbit interactions, under the effects of the EIMF characteristics, can be used to build two-spin-qubit correlations. The considered Hamiltonian is written as

$$\hat{H} = \sum_{i=x,y,z} J_i \hat{\sigma}_A^i \hat{\sigma}_B^i + \sum_{i=x,y} D_i \hat{C}_i + (B_m + b_m) \hat{\sigma}_A^x + (B_m - b_m) \hat{\sigma}_B^x. \quad (2)$$

The time evolution of the two spin-qubits' nonlocal correla-

tions (NCs) will be explored by using Milburn intrinsic decoherence model [48], which is given by

$$\frac{d}{dt} \hat{M}(t) = -i[\hat{H}, \hat{M}] - \frac{\gamma}{2} [\hat{H}, [\hat{H}, \hat{M}]], \quad (3)$$

$\hat{M}(t)$ is the density matrix of the generated two-spin-qubits state. γ is the intrinsic spin-spin decoherence (ISSD) coupling.

Here, the two-spin-qubits eigenvalues V_k ($k = 1, 2, 3, 4$) and the eigenstates $|V_k\rangle$ of the Hamiltonian of Eq. (2) will be calculated, numerically. And hence, in the two-spin-qubits basis: $\{|1_A 1_B\rangle, |1_A 0_B\rangle, |0_A 1_B\rangle, |0_A 0_B\rangle\}$, the two-spin-qubits state dynamics can obtained numerically by using the solution of Eq. (3) giving by

$$\hat{M}(t) = \sum_{m,n=1}^4 U_{mn}(t) S_{mn}(t) \langle V_m | \hat{M}(0) | V_n \rangle |V_m\rangle \langle V_n|. \quad (4)$$

The unitary interaction $U_{mn}(t)$ and the ISSD coupling $S_{mn}(t)$ effects are controlled by the following terms:

$$\begin{aligned} U_{mn}(t) &= e^{-i(V_m - V_n)t}, \\ S_{mn}(t) &= e^{-\frac{\gamma}{2}(V_m - V_n)^2 t}. \end{aligned} \quad (5)$$

The Eq.(4) is used to calculate and explore, numerically, the dynamics of the nonlocal correlations residing within the two-spin-qubits states' Heisenberg XYZ model under the effects of the x, y -spin-orbit interactions (spin-orbit interactions acting along the x - and y - directions) and an applied external magnetic field applying along x -direction.

III. NON-LOCAL CORRELATION (NLC) QUANTIFIERS

Here, the two-spin-qubits' NLCs will be measured by the following LQFI, LQU, and logarithmic negativity (LN):

• LQFI

LQFI can be used as a two-spin-Heisenberg-XYZ correlation quantifier beyond entanglement, which is recently introduced as another correlation type. After calculating the two-spin eigenvalues π_k ($k = 1, 2, 3, 4$) and the two-spin eigenstates $|\Pi_k\rangle$ of Eq. (4) having the representation matrix: $M(t) = \sum_m \pi_m |\Pi_m\rangle \langle \Pi_m|$ with $\pi_m \geq 0$ and $\sum_m \pi_m = 1$, the LQFI is calculated by using the closed expression [34, 37, 38] giving by

$$F(t) = 1 - \pi_R^{\max},$$

π_R^{\max} represents the highest eigenvalue of the symmetric matrix $R = [r_{ij}]$. Based on the Pauli spin- $\frac{1}{2}$ matrices σ^i ($i = 1, 2, 3$) and the elements $\xi_{mn}^i = \langle \Pi_m | I \otimes \sigma^i | \Pi_n \rangle$, the symmetric matrix elements r_{ij} are given by

$$r_{ij} = \sum_{\pi_m + \pi_n \neq 0} \frac{2\pi_m \pi_n}{\pi_m + \pi_n} \xi_{mn}^i (\xi_{nm}^j)^{\dagger}.$$

For a two-spin-qubits maximally correlated state, the LQFI function has $F(t) = 1$. The case of $0 < F(t) < 1$ means that the states have partial LQFI's nonlocal correlation.

- **LQU**

LQU of Wigner–Yanase (WY) skew information [33] is realized to use as an another type of two spin-qubits’ nonlocal correlations [33, 35, 36]. For the two spin-qubits’ density matrix $M(t)$ of Eq. (4), the LQU can be calculated by [35]

$$U(t) = 1 - \lambda_{max}(\Lambda_{AB}), \quad (6)$$

λ_{max} designs the largest eigenvalue of the 3x3-matrix $\Lambda = [a_{ij}]$, which have the elements:

$$a_{ij} = \text{Tr}\{\sqrt{M(t)}(\sigma_i \otimes I)\sqrt{M(t)}(\sigma_j \otimes I)\}.$$

- **Logarithmic negativity (LN)**

We employ the logarithmic negativity [23] to measure of the generated two-spin-qubits entanglement. The LN expression is based on the negativity’s definition μ_t [23] (which is defined as the absolute sum of the matrix’s negative eigenvalues $(M(t))^T$ of the partial transposition of the two spin qubits density matrix $M(t)$ of Eq. (4). The LN can be expressed as:

$$N(t) = \log_2[1 + 2\mu_t], \quad (7)$$

The $N(t) = 0$ for a disentangled two-spin state, $N(t) = 1$ for a maximally entangled two-spin state, and $0 \leq N(t) \leq 1$ for a partially entangled two-spin state.

IV. TWO SPIN-HEISENBERG-XYZ-QUBITS DYNAMICS

Here, we will explore the role of J_α -spin-spin interactions supported by x, y -spin-orbit interactions in the generation dynamics of the two-qubit non-local correlations (of LQFI, local LQU, and LN’s entanglement general Heisenberg-XYZ (non-X)-states in the presence of an x -direction EIMF. To explore the generation of the two-spin-qubits non-local correlations, we consider that the two spins are initially in their uncorrelated upper states $|1_A\rangle \otimes |1_B\rangle$, which its density matrix has no nonlocal correlations of the considered quantifiers. Our focus is on the J_α -spin-spin interaction effects (D_x and D_y), and inhomogeneous x -direction magnetic field parameters (B_m and b_m) in the presence of the intrinsic spin decoherence (ISSD) coupling.

As our first analysis, we display the dynamics of the two spin qubits nonlocal correlations of the LQFI, LQU, and LN, generating due to the couplings $(J_x, J_y, J_z) = (0.8, 0.8, 0.8)$ supported by different intensities of x, y -spin-orbit interactions in the presence of the inhomogeneous x -direction magnetic field having weak uniformity and inhomogeneity $(B_m, b_m) = (0.3, 0.5)$. In the absence of the intrinsic spin-spin decoherence $\gamma = 0$ and the x, y -spin-orbit interactions $(D_x, D_y) = (0.0, 0.0)$, the Fig.1(a) illustrates that the two-spin-qubits LQFI, LQU, and log-negativity grow to reach their maximum. The nonlocal correlations of the LQFI, LQU, and log-negativity undergo slow quasi-regular oscillations having the same frequencies and different amplitudes. LQFI

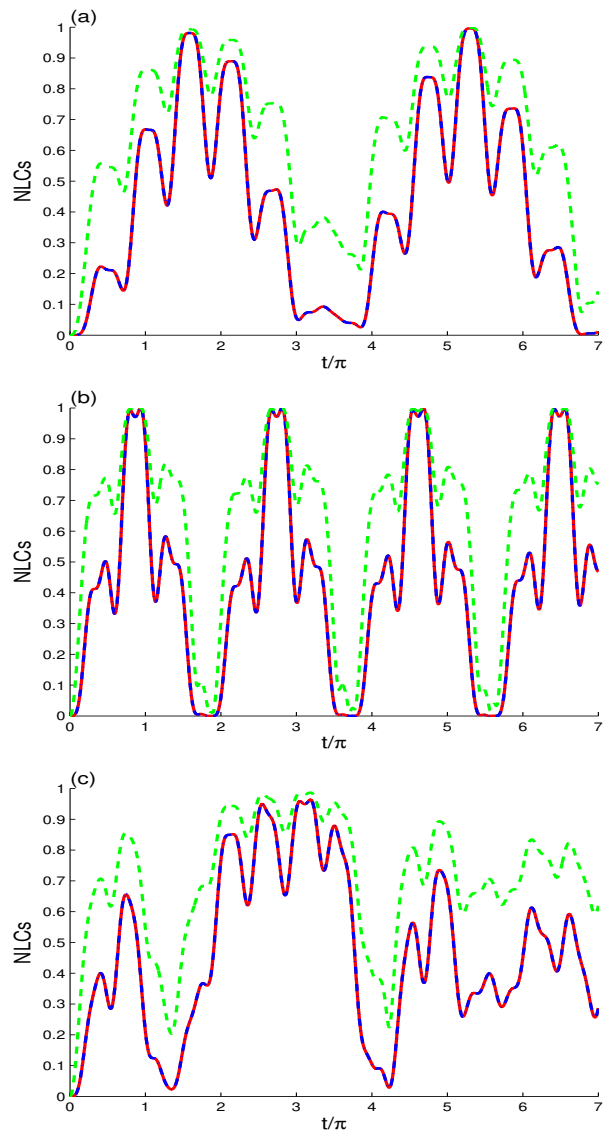


FIG. 1. The dynamics of the generated local-QFI, local-QU, and log-negativity correlations due to the couplings $(J_\alpha, J_y, J_z) = (0.8, 0.8, 0.8)$ are shown under the effects of the applied magnetic field $(B_m, b_m) = (0.3, 0.5)$ and the $D_{x,y}$ interactions: $(D_x, D_y) = (0.0, 0.0)$ in (a), $(D_x, D_y) = (0.5, 0.0)$ in (b), and $(D_x, D_y) = (0.5, 0.5)$ in (c).

and LQU have the same behavior, i.e., the two-spin-qubits correlation is called the “Fisher-Wigner–Yanase nonlocal correlation”. The log-negativity amplitude is always greater than those of the LQFI and LQU. Under these circumstances of weak coupling regime of $J_\alpha = 0.8$ and the applied inhomogeneous x -direction magnetic field (weak uniformity and inhomogeneity), the initial pure-uncorrelated two-spin state undergoes different time-dependent partially correlated states, except particular time, it transforms maximally correlated states. The two-spin states have maximal correlations of Fisher-Wigner–Yanase nonlocal correlation $(F(t) = U(t) = 1)$ and log-negativity $N(t) = 1$ at the same

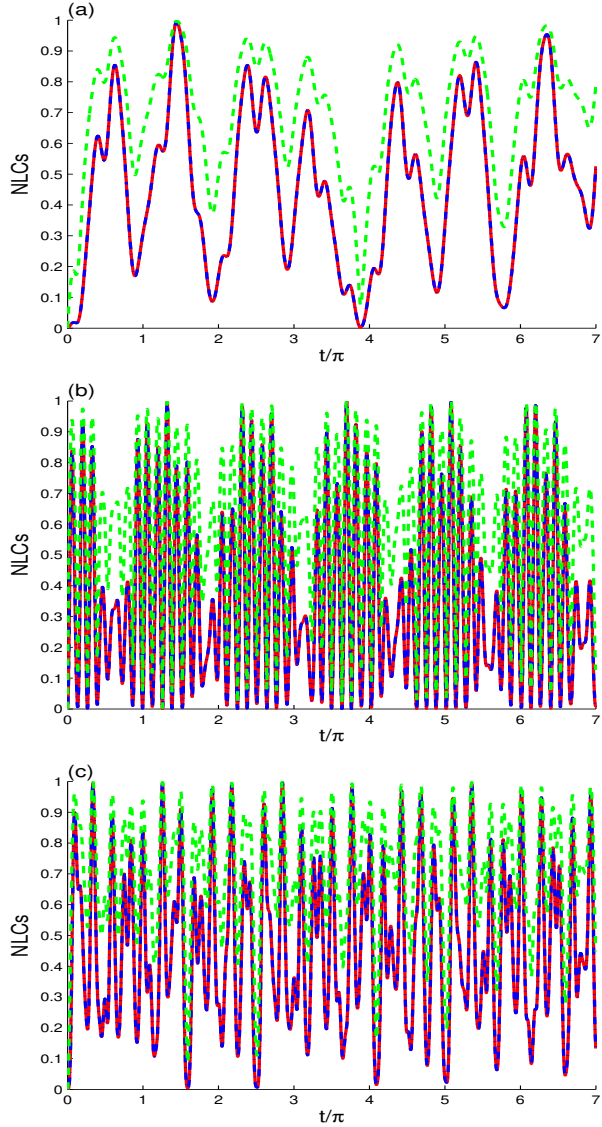


FIG. 2. The LQFI (red solid curve), LQU (blue dash-dotted curve), and log-negativity (green dashed curve) dynamics of Fig.1c are plotted for different Heisenberg-XYZ couplings: $(J_x, J_y, J_z) = (1, 0.5, 1.5)$ in (a) and $(J_x, J_y, J_z) = (5, 1, 1.5)$ in (b), and strong x, y -spin-orbit interactions $D_x = D_y = 2$ in (c).

time. At particular times, we observe that partially two-spin entangled states have no LQFI or LQU correlation.

The effects of weak intensities of x, y -spin-orbit interactions are shown in Fig.1(b). As is clear in this figure, the regularity and fluctuations of the generated Fisher-Wigner-Yanase and log-negativity nonlocal correlations are substantially more than previously presented in the absence of the x, y -spin-orbit interaction. The weak D_x -spin-orbit interaction $(D_x, D_y) = (0.5, 0)$ dramatically improves the appearance of the intervals of the maximal Fisher-Wigner-Yanase and log-negativity nonlocal correlations, as well as the intervals in which two-spin entangled states have no LQFI or LQU correlation. In Fig.1(c), we combined the

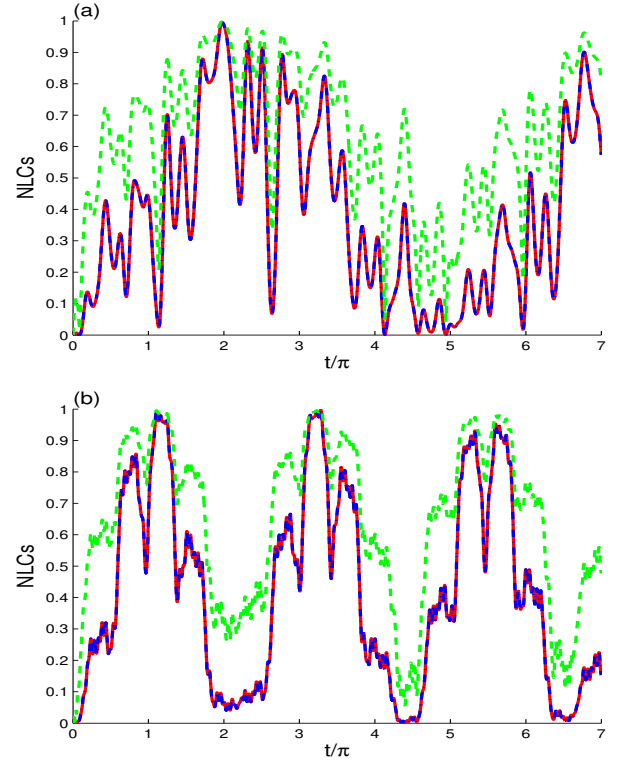


FIG. 3. The LQFI (red solid curve), LQU (blue dash-dotted curve), and log-negativity (green dashed curve) dynamics of Fig.2a (for $(J_x, J_y, J_z) = (1, 0.5, 1.5)$, $(B_m, b_m) = (0.3, 0.5)$, and $D_x = D_y = 0.5$) are plotted for different large magnetic-field uniformities: $B_m = 2$ in (a) and $B_m = 10$ in (b).

D_x - and D_y -spin-orbit interactions $(D_x, D_y) = (0.5, 0.5)$ into x, y -spin-orbit interactions. As is clear in this figure, the NLC fluctuations between their partial and maximal values are substantially fewer than previous results in Figs.1(a,b). Furthermore, the NLC frequency has been reduced while the lower bounds of the Fisher-Wigner-Yanase and log-negativity nonlocal correlations are shifted up. This means that the combined D_x - and D_y -spin-orbit interactions $(D_x, D_y) = (0.5, 0.5)$ improves the generated partial two-spin-qubits Fisher-Wigner-Yanase and log-negativity correlations.

Fig.2 shows that the higher couplings of J_α -spin-spin interactions and x, y -spin-orbit interactions $((J_x, J_y, J_z) = (1, 0.5, 1.5)$ in (a) and $(J_x, J_y, J_z) = (5, 1, 1.5)$ in (b), and strong $D_{x,y}$ -spin-orbit interaction $D_x = D_y = 2$ in (c)) have a high ability to enhancing the arisen two-spin-qubits' NLC of the Fisher-Wigner-Yanase and log-negativity. By comparing the generated spin-spin NLCs showing in Figs.1(c) and 2(a), we find that the relative strong couplings of J_α -spin-spin interactions $(J_x, J_y, J_z) = (1, 0.5, 1.5)$ (which are supported by a weak $D_{x,y}$ -spin-orbit interactions $(D_x, D_y) = (0.5, 0.5)$) increases the amplitudes and frequencies of the Fisher-Wigner-Yanase and log-negativity's oscillations. Fig.2 shows that the higher J_α -couplings lead to the spin-spin NLCs' oscillations have more regu-

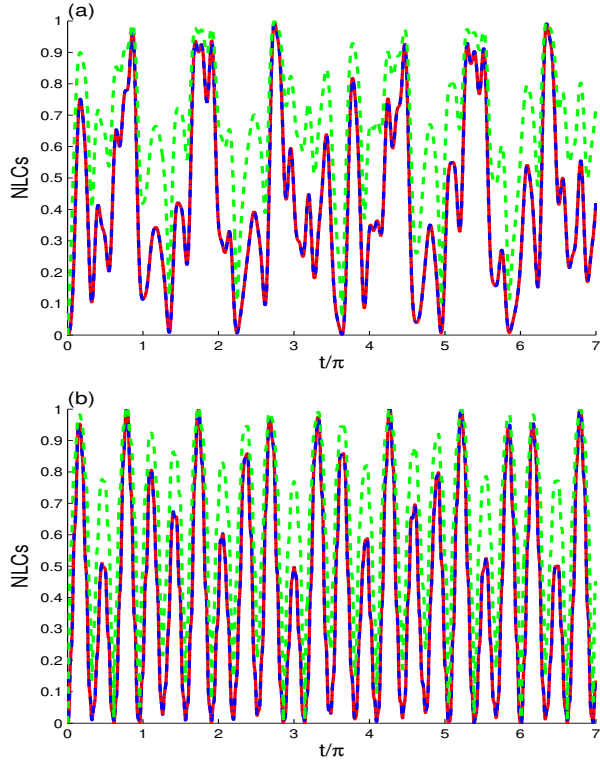


FIG. 4. The LQFI (red solid curve), LQU (boule dash-dotted curve), and log-negativity (green dashed curve) dynamics of Fig.2a (for $(J_x, J_y, J_z) = (1, 0.5, 1.5)$, $(B_m, b_m) = (0.3, 0.5)$, and $D_x = D_y = 0.5$) are plotted for different large magnetic-field inhomogeneities: $b_m = 2$ in (a) and $b_m = 10$ in (b).

larity and fluctuations. The time positions of the maximal Fisher-Wigner-Yanase and log-negativity correlations are enhanced. Fig.2(c) is plotted to see the capability the increase of the x, y -spin-orbit interactions $D_x = D_y = 2$ supporting by weak spin-spin interactions $J_\alpha = 0.8$) to enhance the generated spin-spin NLCs when the external magnetic field applied with weak determinants $(B_m, b_m) = (0.3, 0.5)$. By comparing the qualitative dynamics of the generated Fisher-Wigner-Yanase and log-negativity correlations shown in Fig.1c ($D_x = D_y = 0.5$) with that shown in Fig.2c ($D_x = D_y = 2$), we can deduce that the $D_{x,y}$ -spin-orbit interactions have a high role in enhancement the generated Fisher-Wigner-Yanase and log-negativity correlations, their amplitudes are increased and their oscillations have more fluctuations between their extreme values. In addition, the strong x, y -spin-orbit interactions potentially strength and speed the generation of the Fisher-Wigner-Yanase and log-negativity correlations, due to the J_α -spin-spin interactions.

Figures 3 show Fisher-Wigner-Yanase and log-negativity nonlocal correlation dynamics of Fig.2a (where $(J_x, J_y, J_z) = (1, 0.5, 1.5)$, $b_m = 0.5$, and $D_x = D_y = 0.5$) are plotted for different uniformities of the applied EIMF. Fig. 3a shows the generated Fisher-Wigner-Yanase and log-negativity correlations, due to the J_α -spin-spin and x, y -spin-orbit interactions, previously presented after applying

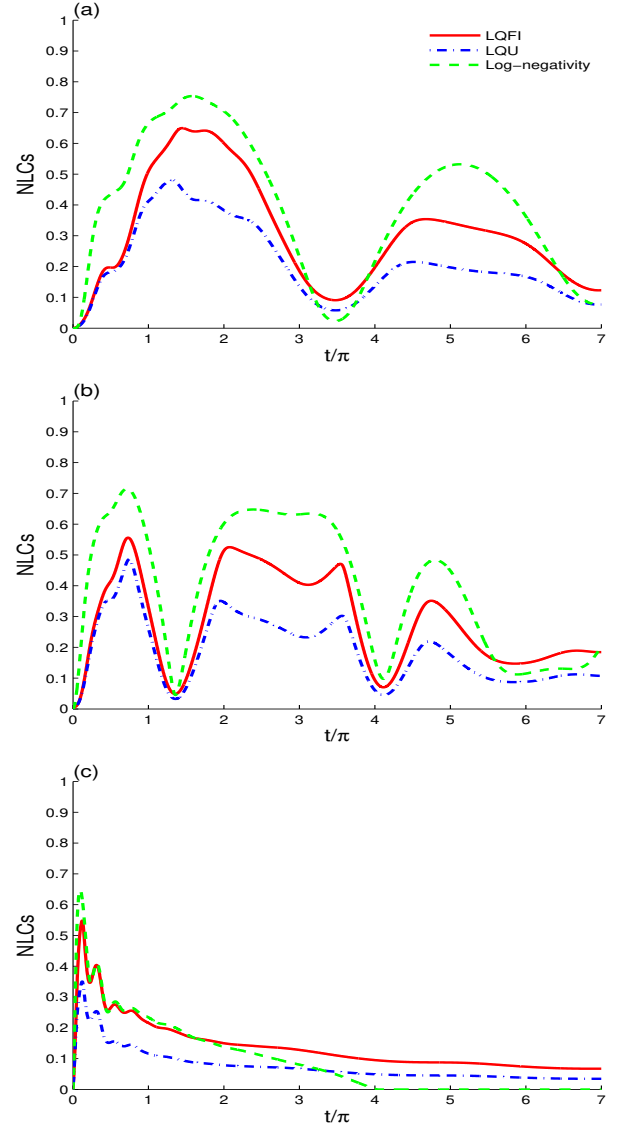


FIG. 5. The LQFI (red solid curve), LQU (boule dash-dotted curve), and log-negativity (green dashed curve) dynamics is shown in the presence of the ISSD $\gamma = 0.05$ and the magnetic field $(B_m, b_m) = (0.3, 0.5)$ with the couplings $J_\alpha = 0.8$ for different couplings: $D_k = 0$ ($k = x, y$) in (a), $D_k = 0.5$ in (b), and $D_k = 2$ in (c).

an external magnetic field (having a small inhomogeneity $b_m = 0.5$ and a large uniformity $B_f = 2$). In this case, the increase of the EIMF uniformity delays the growth of the LQFI, LQU as well as log-negativity. It increases the two-spin state's fluctuations between different partially and maximally correlated states. The generations of the Fisher-Wigner-Yanase and log-negativity correlations shown in Fig.2a (with $B_m = 0.5$) and Fig.3a (with $B_m = 2$) with those shown in Fig.3b (with $B_m = 10$) confirm that the increase of the EIMF uniformity will enhance the ability of the strong J_α -spin-spin interactions supported by weak x, y -spin-orbit interactions to create partially and maximally correlated states with more stability; however, the generated

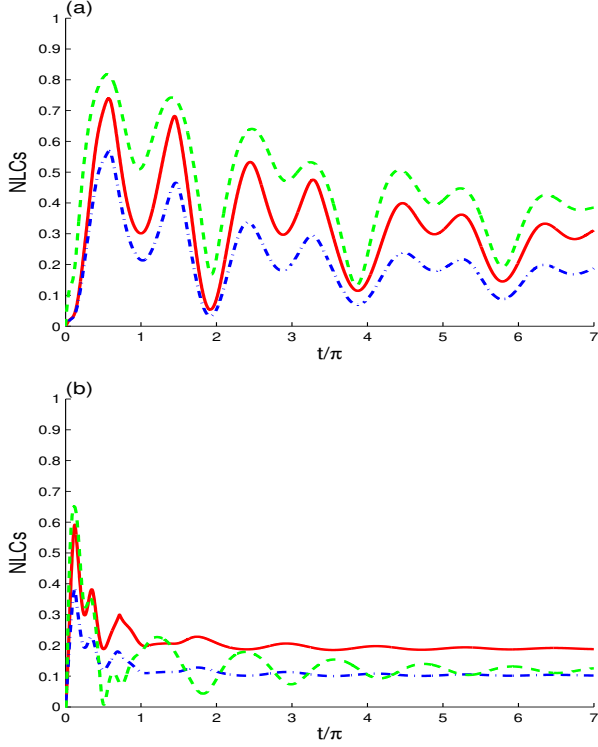


FIG. 6. The two spin-qubits correlation dynamics of the of Fig.5b and c is shown but for strong spin-spin couplings $(J_x, J_y, J_z) = (1, 0.5, 1.5)$.

spin-spin NLCs are more sensitive to the EIMF uniformity.

In the forthcoming analysis of Fig.4, we keep the system with the same parameters' values of Fig.2a (where $(J_x, J_y, J_z) = (1, 0.5, 1.5)$, $B_m = 0.3$, and $D_x = D_y = 0.5$) and consider different magnetic-field inhomogeneities: $b_m = 2$ in (a) and $b_m = 10$ in (b). In this case of Fig.4a, we notice that the larger EIMF uniformities enhance the efficiency of the generation of the Fisher-Wigner-Yanase and log-negativity correlations. The EIMF uniformity increases the two-spin state's fluctuations between different partially and maximally correlated states. The time positions of the maxima ($F(t) = U(t) = N(t) \approx 1$ and minima (zero-value) ($F(t) = U(t) = N(t) \approx 0$) of the generated Fisher-Wigner-Yanase and log-negativity correlations are enhanced. In the case of $(J_x, J_y, J_z) = (1, 0.5, 1.5)$, the increase of the EIMF inhomogeneity have a high role in enhancement the generated two-spin-qubits' NLCs. Where NLCs oscillations' amplitudes and fluctuations are increased (see Fig.4b).

The next illustration of Figs.5-7 is obtained to show the nonlocal correlation dynamics of the LQFI, LQU, and log-negativity in the presence of the non-zero ISSD coupling $\gamma = 0.05$. By comparing the results of Fig.1a ($\gamma = 0.0$) with these of Fig.5a ($\gamma = 0.05$), we find that the LQFI, LQU, and log-negativity shows a decaying oscillatory dynamical evolutions. The generations of the Heisenberg-XYZ (non-X)-states' NLCs (due to $J_\alpha = 0.8$ spin-spin couplings the applied magnetic field $(B_m, b_m) = (0.3, 0.5)$ without spin-orbit

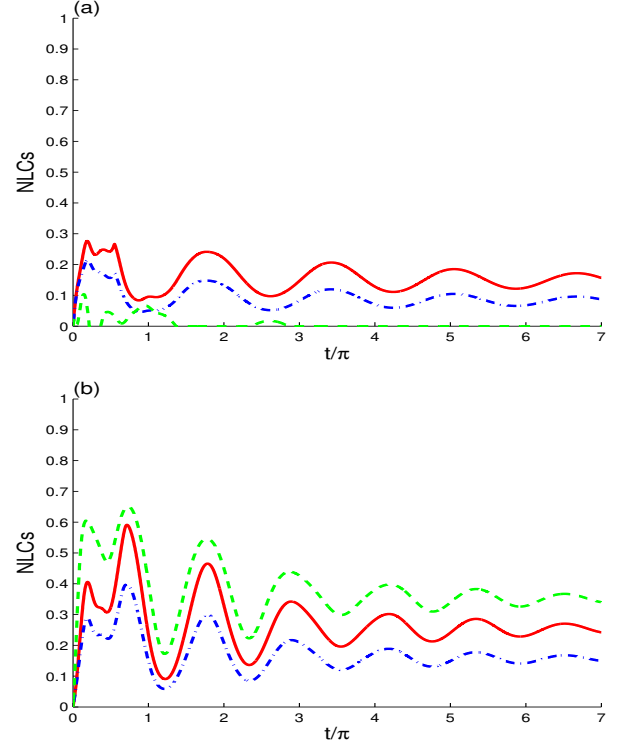


FIG. 7. The dynamics of the LQFI (red solid curve), LQU (boule dash-dotted curve), and log-negativity (green dashed curve) of Fig.3a is shown but for large EIMF's uniformity $(B_m, b_m) = (2, 0.5)$ in (a) and large EIMF's inhomogeneity $(B_m, b_m) = (0.3, 2)$ in (b).

interaction) are weakened and have different amplitudes (which are decreased by increasing the ISSD coupling). After particular interval time, with non-zero ISSD coupling, the LQFI and LQU present different nonlocal correlations having different amplitudes with the same behaviors. Moreover, the NLCs' robustness (against the ISSD effect) of the LQFI and log-negativity is more than that of the LQU.

As shown in Figs.5b and c, the increase of the intensities of x, y -spin-orbit interactions ($D_k = 0$ ($k = x, y$) in (a), $D_k = 0.5$ in (b), and $D_k = 2$ in (c)) reduce the NLCs' robustness (against the ISSD effect) of the LQFI, LQU and log-negativity correlation, the NLCs' amplitudes significantly decrease as the x, y -spin-orbit interactions increase. Moreover, LQFI and LQU display sudden changes at different times. The sudden-changes phenomenon has been studied theoretically [62] and experimentally [63] (see Figs.5b and c). For very strong x, y -spin-orbit interactions $D_k = 2$ (see Fig.5c), we observe that the two-spin-qubits log-negativity drops instantly to zero at a particular time for a long time (sudden-death LN-entanglement phenomenon), then the disentangled two-spin states have only different stable NLCs of the LQFI and LQU. We can deduce that the NLCs' decay resulting from ISSD can be enhanced by increasing the intensities of x, y -spin-orbit interactions.

By comparing the Figs.5(b,c) and Figs.6(b,c), we find that, the strong spin-spin couplings $(J_x, J_y, J_z) = (1, 0.5, 1.5)$ reduce the ISSD effect and improve the NLCs' robustness

(against the ISSD effect) of the LQFI, LQU, and LN. For very strong x, y -spin-orbit interactions $D_k = 2$ (see Fig.6b), the sudden-death LN-entanglement phenomenon does not occur, except at the time $t \approx 0.5\pi$ it occurs instantaneously. The generated two-spin states have different stable partial NLCs of the LQFI, LQU, and LN. In this case, the NLCs' decay resulting from ISSD can be weakened by strengthening the spin-spin interactions.

In the presence of the ISSD effect $\gamma = 0.05$, Fig.7 shows the generated NLCs of the Fig.3a (or it shows the degradation of NLCs of Fig.6a) after strengthening the EIMF's uniformity $(B_m, b_m) = (2, 0.5)$ in (a) and EIMF's inhomogeneity $(B_m, b_m) = (0.3, 2)$ in (b). From Fig.7a, we observe that the large EIMF's uniformity $B_m = 2$ increases the NLCs' decay resulting from ISSD. The time intervals in which the disentangled two-spin states have only different stable NLCs of the LQFI and LQU appeared. Moreover, the NLCs' robustness (against the ISSD effect) of the LQFI and LN is reduced by increasing the large EIMF's uniformity. The outcomes of Fig.7b illustrate that strengthening the EIMF's inhomogeneity $b_m = 2$ also increases the degradation of the NLC functions. In this case of the parameters: $b_m = 2$, $(J_x, J_y, J_z) = (1, 0.5, 1.5)$, and $D_k = 0.5$, we observe that: (1) the generated NLCs (LQFI, LQU and entanglement) of the Fig.3a degrade (due to and ISSD effect) and reach their partial stable oscillatory behaviors, quickly, comparing with the case where the small value of $b_m = 0.5$ of Fig.6a. We find that the ability of the EIMF's inhomogeneity to enhance the ISSD effect is small compared to that of the EIMF's uniformity.

V. CONCLUSION

In this investigation, the Milburn intrinsic decoherence model and Heisenberg XYZ model are used to examine the embedded capabilities in spin-spin interaction and spin-orbit interaction (that describes x, y -DM interactions) to generate nonlocal correlations (realizing by LQFI, LQU, and LN) of general two-spin-qubits (non-X)-states under the effects of the EIMF's uniformity and the inhomogeneity. In the presence and absence of the ISSD, the dependence of the generated nonlocal correlations on the parameters, of spin-spin interaction and spin-orbit interactions as well as of the EIMF's uniformity and the inhomogeneity, are explored. It is found that the spin-spin Heisenberg XYZ and x, y -spin-orbit interactions have a high capability to raise non-local correlations in the presence of a weak external magnetic field. The spin-orbit interactions have a high role in the enhancement of the generated two-spin-qubits Fisher-Wigner-Yanase and log-negativity correlations, their oscillations' amplitudes and fluctuations are increased. In the presence and absence of the ISSD, the NLCs' generations are weakened and have different amplitudes, decreasing by increasing the ISSD coupling. The NLCs' robustness (against the ISSD effect) of the LQFI and log-negativity is more than that of the LQU. The phenomenon of the sudden changes occurs during the LQU and LQFI dynamics whereas the sudden death occurs during log-negativity-entanglement dynamics. The NLCs' decay resulting from ISSD can be enhanced by increasing the intensities of x, y -spin-orbit interactions. Strengthening the spin-spin interactions weakens the NLCs' decay resulting from ISSD. The generated NLCs degrade (due to an ISSD effect with a large IMF's inhomogeneity) and reach their partially stable oscillatory behaviors, quickly. The ability of the IMF's inhomogeneity to increase the ISSD effect is small compared to that of the EIMF's uniformity.

REFERENCES

-
- [1] R. Horodecki, P. Horodecki, M. Horodecki and K. Horodecki, *Rev. Mod. Phys.* **81**, 865 (2009).
 - [2] M. A. Nielsen and I.L. Chuang, *Quantum Computation and Quantum Information*, Cambridge University Press, Cambridge, (2000).
 - [3] D. Loss and D. P. DiVincenzo, *Phys. Rev. A* **57**, 120 (1998).
 - [4] G. Burkard, D. Loss, and D. P. DiVincenzo, *Phys. Rev. B* **59**, 2070 (1999).
 - [5] L. M. K. Vandersypen, R. Hanson, L. H. van Willems Beveren, J. M. Elzerman, J. S. Greidanus, S. De Franceschi, and L. P. Kouwenhoven (2004). *Quantum Computing and Quantum Bits in Mesoscopic Systems*. Springer, Boston, M A.
 - [6] Rong-Long Ma, Ao-Ran Li, Chu Wang, Zhen-Zhen Kong, Wei-Zhu Liao, Ming Ni, Sheng-Kai Zhu, Ning Chu, Chengxian Zhang, Di Liu, Gang Cao, Gui-Lei Wang, Hai-Ou Li, and Guo-Ping Guo *Phys. Rev. Applied* **21**, 014044 (2024).
 - [7] Justyna P. Zwolak and Jacob M. Taylor, *Rev. Mod. Phys.* **95**, 011006 (2023).
 - [8] F. Pinheiro, G. M. Bruun, J.-P. Martikainen, and J. Larson, *Phys. Rev. Lett.* **111**, 205302 (2013).
 - [9] A. Bermudez, L. Tagliacozzo, G. Sierra and P. Richerme, *Phys. Rev. B: Condens. Matter Mater. Phys.* **95**, 024431 (2017).
 - [10] M. Nishiyama, Y. Inada, and Guo-qing Zheng, *Phys. Rev. Lett.* **98**, 047002 (2007).
 - [11] W. Yue, Q. Wei, S. Kais, B. Friedrichc and D. Herschbach, *Phys. Chem. Chem. Phys.* **24**, 25270 (2022).
 - [12] I. Dzyaloshinski, *J. Phys. Chem. Solids* **4**, 241 (1958).
 - [13] T. Moriya, *Phys. Rev.* **117**, 635 (1960).
 - [14] T. Moriya, *Phys. Rev. Lett.* **4**, 228 (1960).
 - [15] L. Shekhtman, O. Entin-Wohlman, A. Aharony, *Phys. Rev. B* **47**, 174 (1993).
 - [16] T. Moriya, *Phys. Rev.* **120**, 91 (1960).

- [17] E. I. Kuznetsova · M. A. Yurischev, *Quantum Inf. Process* **12**, 3587–3605 (2013).
- [18] M. C. Arnesen, S. Bose, and V. Vedral, *Phys. Rev. Lett.* **87**, 017901 (2001).
- [19] D.-C. Li, Z.-L. Cao, *Optics Communications* **282**, 1226–1230 (2009).
- [20] M. Le Bellac, A short introduction to quantum information and quantum computation, Cambridge University Press, Cambridge (2006).
- [21] J. Eisert, M. Cramer, and M. B. Plenio, *Rev. Mod. Phys.* **82**, 277 (2010).
- [22] W. K. Wootters, *Phys. Rev. Lett.* **80** 2245 (1998).
- [23] G. Vidal, R. F. Werner, *Phys. Rev. A* **65**, 032314 (2002).
- [24] F. Eftekhari, M. K. Tavassoly, A. Behjat, M. J. Faghghi, *Optics and Laser Technology* **168**, 109934 (2024).
- [25] M. S. Kheirabady, M. K. Tavassoly, M. Rafeie and E. Ghasemian, *Commun. Theor. Phys.* **76**, 025101 (2024).
- [26] S. L. Braunstein, H. J. Kimble, *Phys. Rev. Lett.* **80** 869 (1998).
- [27] D. Bouwmeester, J. W. Pan, K. Mattle, M. Eibl, H. Weinfurter, A. Zeilinger, *Nature* **390**, 575 (1997).
- [28] Y. Lei, F. K. Asadi, T. Zhong, A. Kuzmich, C. Simon, and M. Hosseini, *Optica*, **10**, 1511-1528 (2023).
- [29] A. K. Ekert, *Phys. Rev. Lett.* **67**, 661 (1991).
- [30] H. Ollivier and W. H. Zurek, *Phys. Rev. Lett.* **88**, 017901 (2001).
- [31] M.-L. Hu, X. Hu, J. Wang, Y. Peng, Y.-R. Zhang and H. Fan, *Phys. Rep.* **762**, 1 (2018).
- [32] A.-B.A. Mohamed and N. Metwally, *Quant. Inf. Process.* **18**, 79 (2019).
- [33] E. P. Wigner, M. M. Yanase, *Proc. Natl. Acad. Sci.* **49**, 910 (1963).
- [34] D. Girolami, A. M. Souza, V. Giovannetti, T. Tufarelli, J.G. Filgueiras, R. S. Sarthour, D.O. Soares-Pinto, I. S. Oliveira, G. Adesso, *Phys. Rev. Lett.*, **112**, 210401 (2014).
- [35] D. Girolami, T. Tufarelli, G. Adesso, *Phys. Rev. Lett* **110**, 240402 (2013).
- [36] S.-X. Wu, J. Zhang, C.-S. Yu and H.-S. Song, *Phys. Lett. A* **378**, 344 (2014).
- [37] H. S. Dhar, M.N. Bera, G. Adesso, *Phys. Rev. A* **991**, 032115 (2015).
- [38] S. Kim, L. Li, A. Kumar, J. Wu, *Phys. Rev. A.* **97**, 032326 (2018).
- [39] C.W. Helstrom, Quantum Detection and Estimation Theory (Academic, New York, 1976).
- [40] M. G. A. Paris, *Int. J. Quant. Inf.* **7**, **125**, (2009).
- [41] F. Benabdallah, A. Ur Rahman, S. Haddadi and M. Daoud, *Phys. Rev. E* **106**, 034122 (2022).
- [42] F. Benabdallah, K. El Anouz, A. Ur Rahman, M. Daoud, A. El Allati, and S. Haddadi, *Fortschr. Phys.* **71**, 2300032 (2023).
- [43] S. Elghaayda, Z. Dahbi, & M. Mansour, *Opt Quant Electron* **54**, 419 (2022).
- [44] P-F. Wei, Q. Luo, H.-Q.-C. Wang, S.-J. Xiong, B. Liu & Z. Sun, *Front. Phys.* **19**, 21201 (2024).
- [45] A. V. Fedorova,, M. A. Yurischev, *Quantum Inf. Process.* **21**, 92 (2022).
- [46] A.-B. A. Mohamed, A. Farouk, M. F. Yassen, and H. Eleuch, *Symmetry* **13**, 2243 (2021).
- [47] A.-B. A. Mohamed, E. M. Khalil, M. M. Selim, and H. Eleuch, *Symmetry* **13** 13, 352 (2021).
- [48] G. J. Milburn: Intrinsic decoherence in quantum mechanics. *Phys. Rev. A* **44**, 5401 (1991).
- [49] M. Qin, Z.-Z. Ren, *Quantum InfProcess* **14**, 2055–2066 (2015).
- [50] S. Mohammad Hosseiny, J. Seyed-Yazdi, M. Norouzi, and P. Livreri, *Sci. Rep.* (2024) **14**, 9607
- [51] A.-B. A. Mohamed, F. M. Aldosari, and H. Eleuch, *Results in Physics***49**, 106470 (2023).
- [52] A. Ait Chlih, N. Habiballah, and M. Nassik, *Quantum Inf Process* **20**, 92 (2021).
- [53] R. Jafari and A. Akbari, *Phys. Rev. A* **101**, 062105 (2020).
- [54] C. Mo, G.-F. Zhang, *Results in Physics* **21**, 103759 (2021).
- [55] V. S. Indrajith, R. Sankaranarayanan, *Physica A* **582**, 126250 (2021).
- [56] A. El Aroui, Y. Khedif, N. Habiballah, M. Nassik, *Opt. and Quantum Elec.* **54**, 694 (2022).
- [57] F. Benabdallah, K. El Anouz, M. Daoud, *Eur. Phys. J. Plus* **137**, 548 (2022).
- [58] N. Zidan, A. Rahman and S. Haddadi, *Laser Phys. Lett.* **20**, 025204, (2023).
- [59] M. A. Yurischev, S. Haddadi, *Phys. Lett. A* **476**, 128868 (2023).
- [60] A.-B. A. Mohamed, *Quantum Inf Process.* **12** 1141 (2013).
- [61] A.-B. A. Mohamed, A. Farouk, M. F. Yassen, and H. Eleuch, *Appl. Sci.* **10**, 3782 (2020).
- [62] J. Maziero, L. C. Celeri, R. M. Serra, and V. Vedral, *Phys. Rev. A* **80**, 044102 (2009).
- [63] J.-S. Xu, X.-Y. Xu, C.-F. Li, C.-J. Zhang, X.-B. Zou, G.-C. Guo, *Nature Commun.* **1**, 7 (2010).